Diverse Functional Motifs within the Three Intracellular Loops of the $CGRP_1$ Receptor†

Alex C. Conner,‡,§ John Simms,‡ Matthew T. Conner,§ Denise L. Wootten,§ Mark Wheatley,§ and David R. Poyner*,‡

School of Life and Health Sciences, Aston University, Birmingham B4 7ET, U.K., and School of Biosciences, University of Birmingham, Birmingham B15 2TT, U.K.

Received August 4, 2006

ABSTRACT: The $CGRP_1$ receptor exists as a heterodimeric complex between a single-pass transmembrane accessory protein (RAMP1) and a family B G-protein-coupled receptor (GPCR) called the calcitonin receptor-like receptor (CLR). This study investigated the structural motifs found in the intracellular loops (ICLs) of this receptor. Molecular modeling was used to predict active and inactive conformations of each ICL. Conserved residues were altered to alanine by site-directed mutagenesis. cAMP accumulation, cell-surface expression, agonist affinity, and CGRP-stimulated receptor internalization were characterized. Within ICL1, L147 and particularly R151 were important for coupling to G_s. R151 may interact directly with the G-protein, accessing it following conformational changes involving ICL2 and ICL3. At the proximal end of ICL3, I290 and L294, probably lying on the same face of an α helix, formed a G-protein coupling motif. The largest effects on coupling were observed with I290A; additionally, it reduced CGRP affinity and impaired internalization. I290 may interact with TM6 to stabilize the conformation of ICL3, but it could also interact directly with Gs. R314, at the distal end of ICL3, impaired G-protein coupling and to a lesser extent reduced CGRP affinity; it may stabilize the TM6−ICL3 junction by interacting with the polar headgroups of membrane phospholipids. Y215 and L214 in ICL2 are required for cell-surface expression; they form a microdomain with H216 which has the same function. This study reveals similarities between the activation of CLR and other GPCRs in the role of TM6 and ICL3 but shows that other conserved motifs differ in their function.

Calcitonin receptor-like receptor (CLR)[1] is a family B G-protein-coupled receptor (GPCR) from the calcitonin receptor subfamily which can form a heterodimer with a single-pass transmembrane protein (RAMP1) to form a functional receptor for the potent vasodilatory neuropeptide, calcitonin gene-related peptide (CGRP). CL/RAMP1 (i.e., the $CGRP_1$ receptor) mediates the actions of CGRP through G_s-stimulated adenylate cyclase activation. We have previously shown the sixth transmembrane domain (TM6) of CLR requires a kink formed by the central proline residue of the helix for a functional CGRP response (*1*). We have also identified two nonconserved polar residues within the second intracellular loop of CLR required for membrane localization (H216) and adenylate cyclase signal transduction (K227) (*2*). No additional information is available concerning the identification of G-protein coupling domains, plasma membrane localization, or agonist-induced internalization for the CGRP receptor; however, several other family B GPCR studies have proposed a crucial role for charged, conserved residues within all three intracellular loops (ICL1, -2, and -3). These include a strictly conserved KL motif vital for G-protein coupling in the human secretin receptor (*3*), the glucagon-like polypetide-1 (GLP-1) receptor (*4*), and the VPAC2 receptor (*5*). There is also a unique basic-X-X-basic motif found in the TM6−ICL3 loop junction which is one of the few functionally relevant and structurally conserved regions shared between the two major families (A and B) of GPCRs (*3*, *6*). Although the basic residues of this motif are the key determinants of function, there is controversy concerning their fundamental role and whether just one or both basic residues together are crucial for receptor function. Within the secretin-like family (B) of GPCRs, the motif often involves both basic residues and is linked with receptor maturation and expression (*3*) as well as signal transduction (*5*). However, the distal basic residue within this region is known to be required directly for signal transduction and/or G-protein interaction of several family A GPCRs (*7*, *8*).

CLR is unusual among GPCRs in requiring accessory proteins for ligand interaction (members of the RAMP

† This work was supported by a grant from the Wellcome Trust to D.R.P. and M.W.

* To whom correspondence should be addressed: School of Life and Health Sciences, Aston University, Birmingham B4 7ET, U.K. Telephone: +44 121 204 3997. Fax: +44 121 359 5142. E-mail: D.R.Poyner@aston.ac.uk.

‡ Aston University.

§ University of Birmingham.

[1] Abbreviations: BSA, bovine serum albumin; CGRP, calcitonin gene-related peptide; CLR, calcitonin receptor-like receptor; DMEM, Dulbecco's modified Eagle's medium; DPPC, dipalmitoylphosphatidylcholine; EDTA, ethylenediaminetetraacetic acid; GLP-1, glucagon-like polypetide-1; GPCR, G-protein-coupled receptor; h, human; HA, hemagglutin; HEPES, 4-(2-hydroxyethyl)-1-piperazineethanesulfonic acid; ICL, intracellular loop; PTH, parathyroid hormone; RAMP, receptor activity-modifying protein; rmsd, root-mean-square deviation; TBS, Tris-buffered saline; TM, transmembrane helix; VIP, vasoactive intestinal polypeptide; WT, wild type.

10.1021/bi0615801 CCC: $33.50
Published on Web 10/11/2006

family) and G-protein coupling (receptor component protein, RCP), and therefore, studies on it are particularly interesting (*9*). The investigation presented here uses molecular mutagenesis techniques in combination with in silico homology modeling to locate and explore the role of proposed structural and functional motifs within the human $CGRP_1$ receptor. We have used molecular modeling to determine the likely spatial arrangement of the intracellular loops in both their active and inactive conformations. We have also constructed a comprehensive series of alanine substitution mutants of all conserved residues within ICL1, -2, and -3. The mutants were analyzed following transient transfection to compare relative cAMP signaling, plasma membrane localization, CGRP affinity, and agonist-mediated internalization. These data highlight two crucial arginyl residues within the first and third intracellular loops (R151 and R314, respectively) and a strictly conserved hydrophobic isoleucine-leucine-leucine face at the TM5−ICL3 junction required for efficient G-protein coupling. The data illustrate that while some elements of GPCR activation are conserved, other motifs can serve a variety of functions.

MATERIALS AND METHODS

Materials. Human αCGRP was from Calbiochem (Beeston, Nottingham, U.K.). Peptides were dissolved in distilled water and stored as aliquots at −20 °C in nonstick microcentrifuge tubes (Thermo Life Sciences, Basingstoke, U.K.). Unless otherwise specified, chemicals were from Sigma or Fisher (Loughborough, U.K.). Cell culture reagents were from Gibco BRL (Paisley, Renfrewshire, U.K.) or Sigma. [^{125}I]Iodohistidyl^8-human αCGRP (2000 Ci/mmol) was from Amersham Biosciences (Chalfont, U.K.).

Expression Constructs and Mutagenesis. Human CL with an N-terminal hemagglutinin (HA) epitope tag (YPYDVPDYA) and human RAMP1 were provided by S. M. Foord (GlaxoWellcome, Stevenage, U.K.) and were subcloned into pcDNA3- (Invitrogen, Renfrew, U.K.) prior to mutagenesis. Introduction of the epitope makes essentially no difference to the pharmacology of the receptor (*10*).

Mutagenesis was carried out using the Quick Change site-directed mutagensis kit (Stratagene, Cambridge, U.K.), following the manufacturer's instructions. Forward and reverse oligonucleotide primers were designed with single-base changes to incorporate amino acid point mutations to alanine in the final CL protein and to engineer restriction sites to aid screening of mutants. The primers were synthesized by Invitrogen. The numbering of the residues assumes a 22-amino acid signal protein prior to the start of the mature transcript (*11*).

Plasmid DNA was extracted from the cultures using a Wizard-Prep DNA extraction kit according to the manufacturer's instructions (Promega, Southampton, U.K.). The plasmid DNA was eluted in 100 μL of sterile distilled water and stored at −20 °C. Sequences were confirmed by sequencing (Functional Genomics, Birmingham, U.K.).

Cell Culture and Transfection. Cos-7 cells were cultured in Dulbecco's modified Eagle's medium (DMEM) supplemented with 10% (v/v) foetal bovine serum and 5% (v/v) penicillin/streptomycin in a humidified 95% air/5% CO_2 atmosphere. For transfection, the cells were plated onto either 12- and 48-well plates or 100 mm dishes. Cells were transfected using a mixture (per 1 μg DNA) of 6 μL of 10 mM polyethyleneimine and 45 μL of a 5% glucose solution incubated for 30 min at room temperature and added to an appropriate final volume of full media; 12- and 48-well plates were treated with 1 μg of DNA per well, and 100 mm dishes were treated with 10 μg of DNA per dish. Characterization of expressed receptors was performed 48−72 h after transfection. A 1:1 RAMP1:CLR DNA ratio was used for transfections.

Membrane Preparation. The cells from each 100 mm plate were washed briefly with 1 mL of cold phosphate-buffered saline and scraped into a small volume of buffer [20 mM HEPES, 2 mM $MgCl_2$, and 1% (w/v) bovine serum albumin (BSA) (pH 7.5)]. The cells were homogenized using an Ultra Turrax homogenizer (full speed for 20 s). The cells were then centrifuged at 20000*g* for 30 min at 4 °C. The supernatant was removed, and the pellets were resuspended in 14 mL of buffer (as before) and used immediately for binding studies or stored at −70 °C.

Radioligand Binding. Membranes were homogenized briefly before being used, and 500 μL was incubated with 100 pM [^{125}I]iodohistidyl^8-human αCGRP and appropriate dilutions of human αCGRP for 60 min at room temperature. Nonspecific binding was assessed in the presence of 1 μM CGRP. The samples were then centrifuged at 12000*g* in a benchtop microcentrifuge for 5 min at room temperature. The pellets were washed twice with water, and the radioactivity was counted in a γ counter.

Assay of cAMP Production. Growth medium was removed from the cells and replaced with DMEM containing 500 μM isobutylmethylxanthine for 30 min. αCGRP in the range 1 pM to 1 μM was added for a further 15 min. All dilutions were carried out in buffer containing 0.1% bovine serum albumin using "NoStick" microcentrifuge tubes (Scientific Specialities Inc., Lodi, CA). Ice-cold ethanol (95−100%, v/v) was used to extract cAMP which was subsequently measured with a radioreceptor assay as previously described (*12*).

Analysis of Cell-Surface Expression of Mutants with an Enzyme-Linked Immunosorbant Assay (ELISA). Cells in 12-well plates were transiently transfected with wild-type (WT) or mutant HA epitope-tagged human CLR and/or RAMP1. The transfected cells were treated with 3.7% formaldehyde for 15 min after aspiration of the growth medium. The cells were then washed three times with 0.5 mL of Tris-buffered saline (TBS). Nonspecific binding of the antibody was blocked with 1% BSA in TBS for 45 min. The cells were treated with 250 μL of primary antibody [mouse, anti-HA antibody 12CA5 (Sigma) diluted 1:1000 in TBS with 1% BSA] for 1 h, and the cells were washed again three times with 0.5 mL of TBS. A further block step was performed for 15 min before the cells were incubated with 250 μL of secondary antibody [anti-mouse, horseradish peroxidase-conjugated antibody (Sigma) diluted 1:1000 in TBS] for 1 h. The cells were washed a further three times before development with OPD tablets (Bio-Rad, Hemel Hempstead, U.K.) according to the manufacturer's instructions. Reactions were terminated with 100 μL of 2 N H_2S0_4 per well. The absorbance measured by the ELISA showed a linear dependence on the DNA concentration used in the transfection.

Analysis of CGRP-Mediated Internalization. Cells in eight wells of a 24-well plate were transiently transfected with WT or mutant HA epitope-tagged human CLR and a RAMP1

construct, as well as a RAMP1-alone control transfection. Four wells for each transfection were treated with 100 nM CGRP (final concentration) for 1 h. Cells were then treated exactly as described above for the ELISA (using appropriate volume reductions for well size). The absorbance (490 nm) measured by the ELISA was normalized for each transfection giving an agonist-mediated percentage decrease in cell-surface expression (% internalization). Mutants with discrepant internalization were examined further using a time course assay under the same conditions that were described.

TM Prediction. Individual TM helix prediction of 58 diverse family B GPCR sequences was performed using the web-based versions of TMHMM2 (*13*) and HMMTOP2 (*14*). A consensus prediction for the boundaries of TMIII and TMIV was generated by visual inspection, and from this initial survey, a CLUSTALW (*15*) profile alignment (using the Blosum matrix) was created against 58 peptide hormone family A GPCRs. The resulting alignment was used to generate an initial homology-based model using the high-resolution X-ray crystal structure of bovine rhodopsin as a template. Further refinement of the homology model was achieved through molecular dynamics (MD) simulations of the receptor embedded in a dipalmitoylphosphatidylcholine bilayer. A series ($n = 5$) of 5 ns MD simulations were carried out using the GROMOS96 force field parameter set, with minor modifications, as implemented in GROMACS (*16*). The resulting trajectories were concatenated and used to produce the final refined model of the CLR. The active state of the CLR was achieved through the use of a modified rhodopsin template which was consistent with experimentally derived distance restraints obtained from the literature (*17*−*21*). Homology models of the active CLR were refined through the use of MD simulations as described above.

Ab Initio Prediction of the ICL Regions of the CLR. RAPPER (*22*) was used to predict ab initio the conformations of ICL1 and -3 from rhodopsin and the CLR. Briefly, 1000 loop backbone conformations were generated using RAPPER assuming idealized stereochemistry for all heavy atoms (N, Cα, C, and O). The side chain orientations for the predicted backbone conformations were modeled using SCWRL (*22*) within the environment of the remaining, nonmodeled protein. Generated fragments were initially scored using an all-atom statistical potential (scop-e4-allatoms-xray-scores scoring set) as described by Samudrala and Moult (*23*). The ensemble of loop conformations was filtered on the basis of a RADPF score such that no more than the top 50 models were retained for energy minimization. Minimization was performed using a l-BFGS minimization method which utilized the AMBER all-atom force field (parm99) together with the Still GB/SA solvation model, as implemented in TINKER (*24*). Minimization was performed until either convergence or a 0.1 kcal/mol cutoff point was reached. Only atoms belonging to either the loop region or the N- or C-terminal anchor residues were allowed to move during minimization. Minimized fragments were subsequently ranked according to the conformational free energy of the loop.

Data Analysis. Curve fitting was done with PRISM Graphpad 4 (Graphpad Software Inc., San Diego, CA). For cAMP studies, the data from each concentration−response curve were fitted to a sigmoidal concentration−response curve to obtain the maximum response, the Hill coefficient, and −log EC_{50} (pEC_{50}). For radioligand binding experiments, curves were fitted to obtain maximum and minimum amounts of binding, the Hill coefficient, and −log IC_{50} (pIC_{50}). As the radioligand was present at concentrations well below its K_d, the IC_{50} values were effectively identical to the K_i values. To estimate B_{max} values with [^{125}I]CGRP, the data were fitted to a sigmoidal curve, calculating the amount bound from the specific activity of the radioligand (this was progressively reduced by dilution with unlabeled CGRP). pEC_{50}, pIC_{50}, and B_{max} values were compared with a paired Student's *t*-test. Comparisons were made only between WT and mutant data from concomitantly transfected cells. A control WT experiment was always performed alongside a mutant experiment.

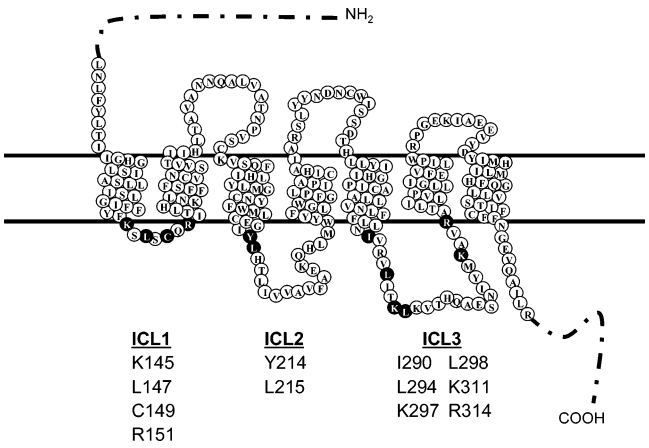

FIGURE 1: Amino acid sequence of the human CLR showing the positions of the mutated residues. The first 22 amino acids of CLR are predicted to form a signal sequence; following the system described in ref *11*, the amino acids are numbered from the start of the predicted mature transcript, E1. Residues with white letters in black circles are highly (>70%) conserved within the three predicted intracellular loops. These residues are listed and were targeted for alanine substitution in this study.

RESULTS

Identification of Conserved Residues within the Boundaries of the ICL Region. As with our previous TM boundary calculations (*2*), the intracellular loop regions comprise K145−R151 (ICL1), L215−M231 (ICL2), and R292−R314 (ICL3). Within these regions, the amino acids strongly conserved within the entire secretin-like family of GPCRs (family B) were identified using the pile-up data from www.gpcrdb.org. Residues that exhibited ∼70% conservation or more were targeted: K145, L147, C149, and R151 from ICL1; Y214 (TM3−ICL2 junction) and L215 from ICL2; and I290A (TM5−ICL3 junction), L294, K297, L298, K311, and R314 from ICL3 (Figure 1). They were clearly distinct from the other residues that exhibited ∼50% or less conservation.

The conserved residues within ICL1, ICL2, and ICL3 of the CLR were mutated individually (or in combination for Y214/L215 and K311/R314) to alanine to identify the contribution to receptor function. Each mutant receptor construct was coexpressed with RAMP1 in Cos-7 cells.

ICL1. The two proximal mutants, K145A and L147A, both resulted in small deleterious effects on CGRP-mediated cAMP accumulation. Although this only reached significance for L147A [3.1-fold reduction; $P < 0.05$ (Figure 2a)], the pEC_{50} value for K145A/L147A was further reduced [9.5-fold (Table 1)], suggesting a role, albeit minor, for K145 in

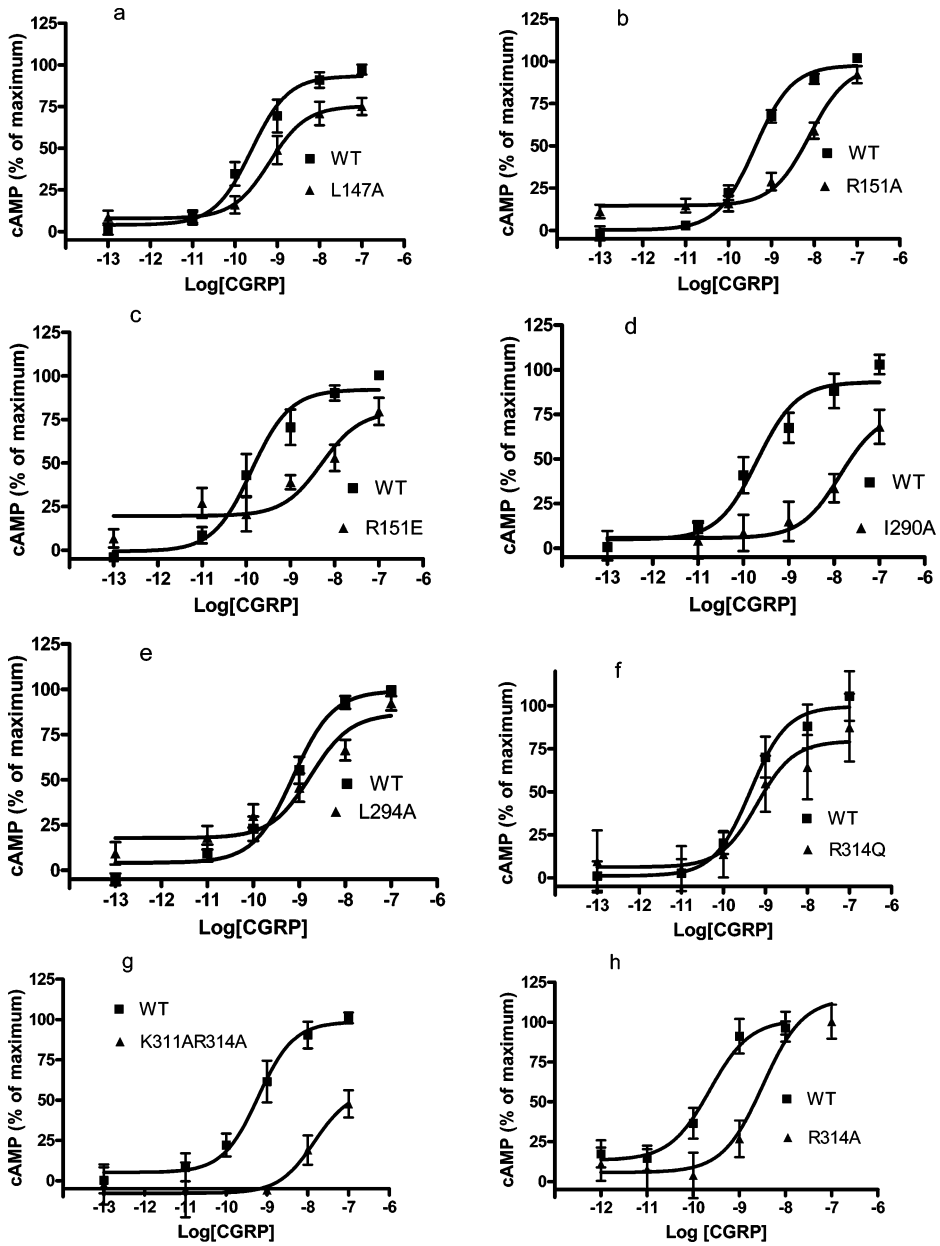

FIGURE 2: CGRP-stimulated cAMP response of the ICL1, -2, and -3 alanine substitution mutants. Cos-7 cells were transfected with WT/RAMP1 or mutant/RAMP1 and assayed for CGRP-stimulated cAMP production: WT receptors (■) and mutant receptors (▲). Data are representative of three to four similar experiments. Points are means ± the standard error of the mean of triplicate points.

coupling to G_s. For L147, there was also a small but significant decrease in the maximum level of cAMP production. C149A had no deleterious effect on CGRP-mediated cAMP accumulation. In contrast, R151A severely disrupted signaling, resulting in a pEC_{50} value increased by more than an order of magnitude compared with the WT value (Figure 2b and Table 1). To determine more precisely the side chain requirements for the R151 position, this residue was substituted with glutamate. This substitution preserves both polarity and approximate chain length while reversing the charge. The pEC_{50} for R151E was reduced to an extent somewhat greater than that seen with R151A (Figure 2c and Table 1). There were no significant changes in CGRP affinity for any mutant (Table 3).

As determined by an ELISA, the cell-surface expression of R151A was similar to that of the wild type (Table 2). K145 exhibited a slightly higher level of expression and L147 a lower level of expression than the wild type. However, the double mutant showed normal expression, and there were no significant differences in the B_{max} values for any of the mutants (Table 3). It seems unlikely that any of the mutants cause major perturbations in receptor expression. The mutants all exhibited wild-type internalization (Table 4).

ICL2. Y214 and L215 were investigated by means of a double mutant (Y214A/L215A). We previously reported that it had no significant deleterious effects on the CGRP-mediated signaling response (*2*; see also Table 1). However, in this study when cell-surface expression was assessed, it was reduced by ~70% (Table 2). Internalization was the same as that of the wild type (Table 4).

ICL3. The largest of the three loop regions, ICL3, has several clear areas of sequence conservation. I290 is proximal to TM5, and the I290A mutation caused a profound perturbation in cAMP accumulation [68-fold reduction in pEC_{50} (Figure 2d and Table 1)]. The signaling of neither K297A nor L298A was significantly different from wild-

Table 1: Functional Parameters of WT/RAMP1 and Mutant Receptors

mutant	WT pEC_{50}[a]	pEC_{50}[a]	fold reduction
K145A	9.62 ± 0.16 (3)	9.39 ± 0.12 (3)	1.70
L147A	9.61 ± 0.37 (6)	9.12 ± 0.45 (6)[b]	3.10[b]
C149A	9.82 ± 0.61 (3)	10.18 ± 0.61 (3)	0.44
R151A	9.47 ± 0.16 (6)	8.15 ± 0.42 (6)[c]	20.8[c]
K145A/L147A	9.52 ± 0.22 (6)	8.54 ± 0.27 (6)[c]	9.55[c]
R151E	9.80 ± 0.33 (6)	8.16 ± 0.38 (6)[c]	43.7[c]
Y214A/L215A	9.17 ± 0.26 (5)	8.71 ± 0.25 (6)	2.88
I290A	9.69 ± 0.18 (6)	7.86 ± 0.38 (6)[c]	67.6[c]
L294A	9.19 ± 0.33 (7)	8.86 ± 0.35 (7)[b]	2.13[b]
K297A	9.23 ± 0.50 (3)	8.95 ± 0.54 (3)	1.91
L298A	9.01 ± 0.18 (6)	8.80 ± 0.15 (6)	1.58
K311A/R314A	9.21 ± 0.25 (6)	7.85 ± 0.39 (6)[b]	22.9[b]
K311A	8.73 ± 0.13 (5)	8.58 ± 0.22 (5)	1.41
R314A	9.65 ± 0.22 (6)	8.43 ± 0.23 (6)[b]	16.6[b]
R314E	9.38 ± 0.42 (4)	9.05 ± 0.44 (4)	2.14
R314Q	9.54 ± 0.16 (6)	9.35 ± 0.22 (6)	1.54

[a] Values are means ± the standard error of the mean; the number of determinations is given in parentheses. The maximum responses (E_{max}) were not significantly different from that for the concomitantly expressed WT receptor for all of the mutants in this study except L147. [b] Value significantly different from that of WT ($p < 0.05$), as assessed by paired *t*-test analyses. [c] Value significantly different from that of WT ($p < 0.01$), as assessed by paired *t*-test analyses.

Table 2: Surface Expression Summary for Mutant Receptors

mutant	Ab_{max}[a]	mutant	Ab_{max}[a]
K145A	152.1 ± 17.8%[b]	I290A	125.4 ± 9.6%
L147A	69.26 ± 10.5%[b]	L294A	98.43 ± 14.1%
C149A	94.71 ± 9.7%	K297A	94.57 ± 17.4%
R151A	96.95 ± 3.8%	L298A	84.11 ± 35.7%
K145A/L147A	126.6 ± 25.7%	K311A/R314A	105.5 ± 32.5%
Y214A/L215A	34.64 ± 6.6%[b]		

[a] Values are means ± the standard error of the mean of at least three determinations. Ab_{max} is the relative cell-surface expression level of receptors as measured by detection of HA tags in an ELISA. Data normalized to WT as 100%. [b] Value significantly different from that of WT ($p < 0.05$), determined via a one-way ANOVA followed by Dunnett's test.

Table 3: Displacement of [^{125}I]CGRP by Unlabeled CGRP at the Functionally Important Mutants Compared to WT

	pIC_{50} (nM)[a]	B_{max} (pmol/mg)
WT	9.03 ± 0.10 (3)	0.33 ± 0.12
K145A	9.06 ± 0.12 (3)	0.17 ± 0.024
L147A	9.17 ± 0.13 (3)	0.18 ± 0.048
R151A	8.72 ± 0.27 (3)	0.63 ± 0.11
I290A	8.32 ± 0.12 (3)[b]	0.43 ± 0.100
L294A	8.87 ± 0.09 (3)	0.22 ± 0.07
K297A	9.08 ± 0.14 (3)	0.39 ± 0.11
L298A	8.91 ± 0.10 (3)	0.37 ± 0.14
K311A/R314A	8.22 ± 0.17 (3)[b]	0.51 ± 0.16
R314A	8.36 ± 0.15 (3)[b]	0.35 ± 0.04

[a] Values are means ± the standard error of the mean; the number of determinations is given in parentheses. [b] Value significantly different from that of WT ($p < 0.05$), determined via a one-way ANOVA followed by Dunnett's test.

type cAMP signaling, but L294A showed a slight but significant reduction in its pEC_{50} value (Figure 2e,f and Table 1). I290A showed a 5-fold decrease in CGRP affinity compared with that of the wild type (Figure 3b and Table 3). The decrease in the magnitude of cAMP signaling for this mutant was significantly more pronounced than the small reduction in CGRP affinity which is, itself, smaller than that seen for the CGRP receptor uncoupled by GppNHp (*1*).

Table 4: CGRP-Stimulated Internalization Compared with Nonstimulated Expression of Wt/RAMP1 and Mutant Receptors

construct	no CGRP[a]	100 nM CGRP	% internalization
WT	100 ± 2.41	38.83 ± 14.95	61.17
K145A	100 ± 5.58	35.67 ± 7.52	64.33
L147A	100 ± 4.89	42.87 ± 7.9	57.13
C149A	100 ± 3.54	37.94 ± 3.79	62.06
R151A	100 ± 2.17	28.81 ± 2.92	71.19
K145A/L147A	100 ± 2.43	45.72 ± 2.69	54.28
Y214A/L215A	100 ± 12.3	45.55 ± 6.93	54.45
I290A	100 ± 3.52	62.90 ± 6.56[b]	37.10[b]
L294A	100 ± 6.23	24.23 ± 3.77	75.77
K297A	100 ± 6.26	29.97 ± 5.24	70.03
L298A	100 ± 3.14	34.46 ± 4.17	65.54
K311A/R314A	100 ± 2.76	39.53 ± 2.62	60.47

[a] Values are means ± the standard error of the mean; the number of determinations is given in parentheses. [b] Value significantly different from that of WT ($p < 0.05$), determined via a one-way ANOVA followed by Dunnett's test.

I290A exhibited a significantly reduced level of internalization compared to that of the wild type (Table 4). Typically, when treated with 100 nM CGRP, ~60% of the wild-type receptors exhibit rapid internalization that reaches a plateau within 1 h. In comparison, only some 30% of 1290A receptors were internalized; this plateau was stable for at least 4 h (Figure 4).

K311 and R314 are conserved residues at the distal end of ICL3 and form a conserved basic-x-x-basic motif. Analysis of the roles of these two amino acids by single and double alanine mutations showed that K311A was identical to wild-type receptors, while the R314A mutation caused a >10-fold reduction in pEC_{50}, an effect approaching that of the double mutant [22.9-fold reduction (Figure 2g,h and Table 1)]. Interestingly, R314E and R314Q had pEC_{50} values that were not significantly different from that of the wild type, suggesting that polarity rather than a full charge is important. R314A also had a small effect on CGRP binding, reducing the affinity by ~5-fold (Table 3); its effect was similar to the reduction noted with K311A/R314A (Figure 3b).

All mutants examined from ICL3 had wild-type receptor expression as judged by ELISA and radioligand binding (Tables 2 and 3). Apart from I290A, all other mutants in ICL3 also had wild-type internalization.

Computer Modeling of Intracellular Regions of CLR. We previously used an ab initio approach to model the CLR, to include the second intracellular loop of the CLR. This successfully predicted the structure of the corresponding structure of the loop as shown by the crystal structure of rhodopsin. We also extended this to model the likely conformation of the loop following receptor activation. For this, we utilized a refined TM helical bundle based on experimentally derived distance constraints which are consistent with an active conformation of bovine rhodopsin (*2*). We used this methodology to predict the structure of ICLs in the inactive and active forms of the receptor. Figure 5a shows the loops in the proposed active and inactive conformations of the receptor. ICL1 appears to undergo very little movement; by contrast, there is considerable movement of ICL2 and -3. This "flowering" arrangement exposes a potential G-protein binding pocket. In ICL1, the side chain of R151 is oriented toward this pocket. By contrast, the side chain of L147 points toward the probable cytoplasmic helix

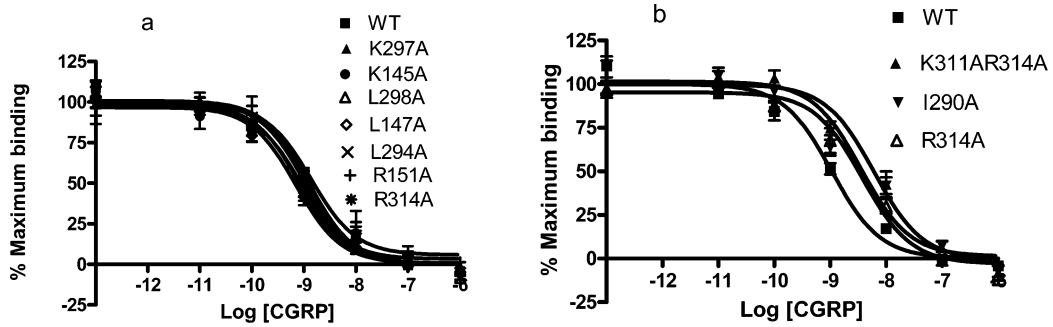

FIGURE 3: Displacement of [^{125}I]CGRP by unlabeled CGRP at the functionally important mutants compared to WT. Cos-7 cells were transfected with WT/RAMP1 or mutant/RAMP1, and membranes were assayed for [^{125}I]CGRP binding. Data are means ± the standard error of the mean of three to four experiments: (a) mutants with no change in binding and (b) I290A, R314A, and K311A/R314A.

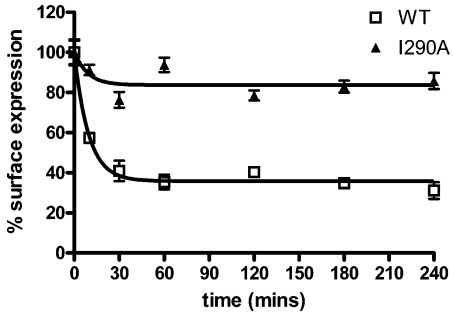

FIGURE 4: Time course internalization curve for I290A. Cos-7 cells were transfected with WT/RAMP1 or I290A/RAMP1 and assayed for cell-surface expression after being exposed to 100 nM CGRP. Data are representative of three to four similar experiments. Points are means ± the standard error of the mean of triplicate points.

8. TM3 is predicted to extend into ICL2 to include both Y215 and L214; they are oriented toward the other TM helices and the ICLs (Figure 5b). In Figure 5c, the proximal end of ICL3 is shown; it can be seen that this is predicted to be helical, with I290 and L294 aligning on the same side. During receptor activation, it is predicted that the fifth transmembrane helix rotates anticlockwise if viewed from the extracellular surface, and there is also movement of the proximal and distal ends of ICL3 toward each other. The distance between the α-carbon atom of I290 and its nearest neighbor on TM6 (V313) shrinks from 10.6 to 6.1 Å. These movements orient I290 and L294 toward the corresponding helical extension of TM6 where the residues could pack against Y308 and M309. However, I290 is also oriented toward the probable G-protein binding pocket (Figure 5d). R314 appears to be located at the membrane interface of TM6 (Figure 5e). During activation, the helix undergoes a lateral translation; however, R314 retains its juxtamembrane location with little vertical displacement.

DISCUSSION

The lack of reliable structural data for any member of the class II GPCRs and the poor sequence homology between this family and rhodopsin [for which there is a crystal structure available (*25*)] limit our ability to identify regions that likely are functionally important. We have combined the results of mutagenesis with molecular modeling in this and previous studies (*1*) to circumvent these problems. The active state model is built using distance constraints measured from activated rhodopsin but also independently observed in the *β*-adrenergic receptor (*27*, *28*). These produce a physically reasonable model of the CLR consistent with experimental data. This approach has identified a number of functionally important regions in the three ICLs and suggested how they might operate. It is important to stress that this modeling is necessarily speculative; there is discussion in the literature about the most physiologically relevant structure of the ICLs as seen in the various crystal structure (*26*), and furthermore, the ICLs in the CLR are significantly longer than in rhodopsin. Nevertheless, the modeling has produced mechanistically plausible explanations for the data which in principle could be tested by techniques such as electron spin resonance.

In rhodopsin, there is evidence for a 2−3 Å movement of the distal portion of TM2 upon light activation, with a corresponding distortion of ICL1 (*20*). By contrast, modeling ICL1 in the CLR suggests that it does not undergo any significant change in conformation following receptor activation; TM2 in the CLR lacks the GG motif found in the corresponding helix in rhodopsin which acts as a hinge. However, L147 and R151 play clear roles in ensuring efficient coupling to G_s. The modeling suggests that R151 is the most likely of these residues to interact directly with G_s, perhaps via an ionic interaction as R151E failed to restore activity. It has been suggested that within family B GPCRs, the equivalent of R151 may represent the central arginine residue in the family A DRY motif (*26*, *27*). For it to be strictly analogous, it would need to form an ionic interaction with a negatively charged counterion in the inactive state of the receptor; E211 in TM3 is a candidate, but further work is needed to establish this. L147 may participate in a hydrophobic interaction, with either the receptor (possibly helix 8 or the bottom of TM7), G_s, or RCP. Loss of coupling at either R151 or L147 was not accompanied by a reduction in CGRP affinity. A similar observation has been noticed for the equivalent arginine residue (R176) of the GLP-1 receptor (*4*). This is consistent with a lack of movement of ICL1 and its corresponding helices; there would be no conformational change to be transmitted to the CGRP binding pocket on the extracellular face of the receptor. There is strong evidence that ICL1 is a contact point for G-proteins in the calcitonin and CRF receptors as splice variants of these receptors with insertions in ICL1 exhibit impaired coupling to G_s (*28*).

C149 has no apparent role in cAMP accumulation or internalization in the CGRP receptor, which was surprising considering the full conservation of this residue within the family B GPCR. Its role, if any, in CLR remains to be determined.

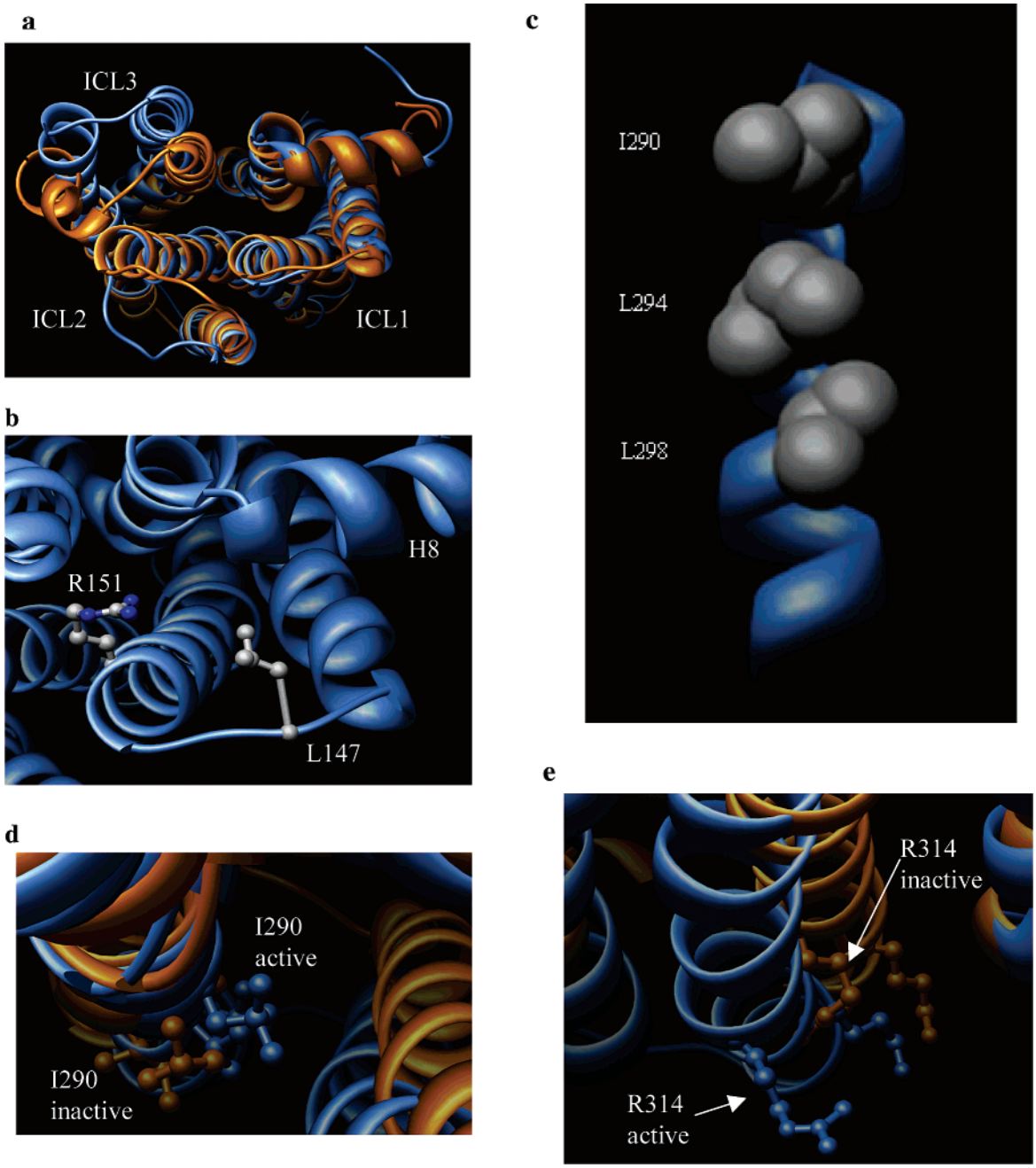

FIGURE 5: Modeling of the CLR. In all figures, the active form of the receptor is colored blue and the inactive form orange. (a) View from the cytoplasmic side showing all three ICL loops. (b) View looking at the cytplasmic surface of ICL1, showing R151 and L147. (c) View of the proximal end of ICL3, showing how it forms a helix with I290, L294, and L298 on one surface. (d) View looking down TM5 from the extracellular surface, showing rotation of I290 during receptor activation. (e) View looking down TM6 from the extracellular surface, showing R314 and K311 (unlabeled residue).

In a previous study of ICL2, it was shown that H216 was required for cell-surface expression (*2*). The study presented here suggests that it is part of motif that includes Y215 and L214. H216 is oriented away from the helical bundle, making it a suitable candidate for interaction with a trafficking protein. The modeling suggests that Y214 and L215 are probably involved in helix packing, perhaps stabilizing the conformation of H216.

ICL3 plays a key role in G-protein recognition in both the A and B families of GPCRs (*29*, *30*). In CLR, this loop has a number of motifs implicated in G-protein interaction. However, there is no consensus about their exact roles (Table 5).

It is well-established that the proximal portion of ICL3 in many family A GPCRs forms an amphipathic α-helix and that this is important in G-protein coupling (*31*). Similar features have been noted in family B GPCRs; a study of the GLP-1 receptor concluded that the hydrophobic face of this helix was involved in G-protein contacts (*4*). With the CLR, the modeling suggests that I290 and L294 participate in this hydrophobic face. In the M5 muscarinic receptor, it has been proposed that the helix stabilizes the wall of the G-protein pocket by packing against the distal portion of ICL3 (*6*); a similar mechanism may be important here for G_s or RCP. In addition to disrupting coupling, I290A reduces CGRP affinity and disrupts receptor internalization; to the best of our knowledge, this residue or its equivalent has not previously been implicated in internalization in other GPCRs. The effects on CGRP binding may be secondary to the

Table 5: Role of ICL Motifs in Other Family B Receptors

CLR residue	motif	receptor	residue	action	ref
C149	ICL1	GLP-1	C174A	reduced level of expression	*4*
R151		GLP-1	R176A	decreased E_{max}, pEC_{50}	
Y214	YL, ICL2	VPAC1	Y239A	small decrease in E_{max}	*37*
L215		VPAC1	L240A	large decrease in E_{max}	
I290	proximal arm ICL3	GLP-1	I522A	decrease in E_{max}, pEC_{50}	*4*
L294		PTH	L379A	reduces IP3 but not cAMP	*36*
K297	KLK, ICL3	secretin	K323I	reduced level of cAMP accumulation	*3*
		GLP1	K334A	reduced pEC_{50}	*39*
		VPAC1	K332A	reduced pK_d and efficacy	*40*
		PTH	K328A	reduced level of cAMP accumulation	*38*
L298		VPAC2	L310A	reduced efficacy, cAMP	*35*
K311	BXXB, ICL3	VPAC1	R338A	WT	*40*
		secretin	R339A	WT	*3*
		GLP-1	R348G	lower pK_d	*41*
		GLP-1	R348A	WT	*39*
		VPAC2	R325A	large decrease in pEC_{50}	*35*
A312		VPAC1	L239A	WT	*40*
		GLP-1	L349A	WT	*39*
V313		GLP-1	A350E,K	very low expression level	
R314		VPAC1	R241A	WT	*40*
		secretin	R342A	WT (but double with R339A abolishes cell-surface expression)	*3*
		GLP-1	K351A	WT	*39*
		VPAC2	R328A	modest decrease in pEC_{50}	*35*

disruption of the G-protein interaction. It is not clear why I290A impairs internalization. It cannot be simply a result of poor coupling to G_s as mutants with a similar degree of coupling impairment (R314 and R151) exhibit normal internalization. An interaction, directly or indirectly with a component of the internalization machinery or arrestin, may be disrupted.

There are a number of other well-conserved motifs within ICL3 that are frequently (but not invariably) involved in G-protein coupling. The KL(K) motif (Table 5) is represented by K297L298 in CLR but is unimportant for G_s coupling in this receptor. The basic-X-X-basic motif can be seen in both family A and B GPCRs, but effects of mutations are variable (Table 5). In the CLR, the effects of the basic-X-X-basic motif seem largely to be due to the influence of R314, perhaps in promoting coupling to G_s. While a hydrophilic substituent is required at this position, a charge is not essential. It is possible that in R314E, the glutamic acid is protonated due to its proximity to the lipid tails of the membrane phospholipids. R314 may be directly involved in G-protein coupling, but the model suggests that the side chain in both the active and inactive states points away from the G-protein binding pocket. It may be required for interaction with another accessory protein such as RCP (*32*). However, as a hydrophilic amino acid, it could help anchor the N-terminal end of TM6 at the level of the plasma membrane, by interacting with the polar headgroups of phospholipids (*33*). The removal of this constraint could destabilize the G-protein binding pocket formed by ICL3. The small effect on CGRP binding affinity seen with this mutant can be explained by assuming that changes in the cytoplasmic end of TM6 are transmitted directly to the third extracellular loop, which is likely to be involved in CGRP binding. We have previously shown that mutation of P321 in the middle of the helix substantially impairs agonist binding (*1*).

It is possible to draw some general conclusions from this and other studies on the CLR (*1*). There are areas of similarity between the activation of CLR and other GPCRs from the A and B families. The movement of TM6 and hence ICL3 is a crucial event in creating a G-protein binding pocket in this and most other GPCRs. In particular, the junction between TM5 and ICL3 seems particularly important for G-protein interactions. By contrast, there is less conservation of function at the distal ends of TM2 and -3. Even within the B family of GPCRs, while motifs may be conserved they can be adapted to distinct functions or become redundant. In the CLR, this is illustrated by the roles (or lack thereof) of the KL and the basic-X-X-basic motifs. To fully understand this variation, it will be necessary to study structures of individual GPCRs complexed with Gα. However, the model of the CLR gives some clues about why this might happen. Only a few residues are likely to be essential for direct interactions with G_s, probably forming charge−charge interactions. The significance of the rest will be highly sequence specific as other amino acids may be able to compensate for removal of an interaction. The expression of a particular phenotype may also be cell line specific; factors such as G-protein concentration or the presence of an accessory protein may either accentuate or mask a difference. For the CLR, the KL motif may be unimportant due to a particularly strong contribution from the preceding hydrophobic face of the TM5−ICL3 interface. Equally, TM6 may be particularly dependent on R314 to anchor it; the role of P321 in this helix shows that its dynamics are different from those of TM6 in some other family B GPCRs such as the VPAC1 receptor (*1*). The CLR also has interactions with RCP and possibly the C-terminus of RAMP1 (*34*) which can modulate the role of conserved motifs, making it a particularly interesting receptor to study.

REFERENCES

1. Conner, A. C., Hay, D. L., Simms, J., Howitt, S. G., Schindler, M., Smith, D. M., Wheatley, M., and Poyner, D. R. (2005) A key role for transmembrane prolines in calcitonin receptor-like receptor agonist binding and signalling: Implications for family B G-protein-coupled receptors, *Mol. Pharmacol. 67*, 20−31.

2. Conner, A. C., Simms, J., Howitt, S. G., Wheatley, M., and Poyner, D. R. (2005) The second intracellular loop of the CGRP-receptor provides molecular determinants for signal transduction and cell-surface expression, *J. Biol. Chem. 281*, 1644−51.
3. Chan, K. Y., Pang, R. T., and Chow, B. K. (2001) Functional segregation of the highly conserved basic motifs within the third endoloop of the human secretin receptor, *Endocrinology 142*, 3926−34.
4. Mathi, S. K., Chan, Y., Li, X., and Wheeler, M. B. (1997) Scanning of the glucagon-like peptide-1 receptor localizes G protein-activating determinants primarily to the N terminus of the third intracellular loop, *Mol. Endocrinol. 11*, 424−32.
5. Hilairet, S., Belanger, C., Bertrand, J., Laperriere, A., Foord, S. M., and Bouvier, M. (2001) Agonist-promoted internalization of a ternary complex between calcitonin receptor-like receptor, receptor activity-modifying protein 1 (RAMP1), and β-arrestin, *J. Biol. Chem. 276*, 42182−90.
6. Hill-Eubanks, D., Burstein, E. S., Spalding, T. A., Brauner-Osborne, H., and Brann, M. R. (1996) Structure of a G-protein-coupling domain of a muscarinic receptor predicted by random saturation mutagenesis, *J. Biol. Chem. 271*, 3058−65.
7. Timossi, C., Ortiz-Elizondo, C., Pineda, D. B., Dias, J. A., Conn, P. M., and Ulloa-Aguirre, A. (2004) Functional significance of the BBXXB motif reversed present in the cytoplasmic domains of the human follicle-stimulating hormone receptor, *Mol. Cell. Endocrinol. 223*, 17−26.
8. Saito, Y., Tetsuka, M., Saito, S., Imai, K., Yoshikawa, A., Doi, H., and Maruyama, K. (2005) Arginine residue 155 in the second intracellular loop plays a critical role in rat melanin-concentrating hormone receptor 1 activation, *Endocrinology 146*, 3452−62.
9. Conner, A. C., Simms, J., Hay, D. L., Mahmoud, K., Howitt, S. G., Wheatley, M., and Poyner, D. R. (2004) Heterodimers and family-B GPCRs: RAMPs, CGRP and adrenomedullin, *Biochem. Soc. Trans. 32*, 843−6.
10. McLatchie, L. M., Fraser, N. J., Main, M. J., Wise, A., Brown, J., Thompson, N., Solari, R., Lee, M. G., and Foord, S. M. (1998) RAMPs regulate the transport and ligand specificity of the calcitonin-receptor-like receptor, *Nature 393*, 333−9.
11. Koller, D., Born, W., Leuthauser, K., Fluhmann, B., McKinney, R. A., Fischer, J. A., and Muff, R. (2002) The extreme N-terminus of the calcitonin-like receptor contributes to the selective interaction with adrenomedullin or calcitonin gene-related peptide, *FEBS Lett. 531*, 464−8.
12. Poyner, D. R., Andrew, D. P., Brown, D., Bose, C., and Hanley, M. R. (1992) Pharmacological characterization of a receptor for calcitonin gene-related peptide on rat, L6 myocytes, *Br. J. Pharmacol. 105*, 441−7.
13. Krogh, A., Larsson, B., von Heijne, G., and Sonnhammer, E. L. (2001) Predicting transmembrane protein topology with a hidden Markov model: Application to complete genomes, *J. Mol. Biol. 305*, 567−80.
14. Tusnady, G. E., and Simon, I. (2001) The HMMTOP transmembrane topology prediction server, *Bioinformatics 17*, 849−50.
15. Wilbur, W. J., and Lipman, D. J. (1983) Rapid Similarity Searches of Nucleic Acid and Protein Data Banks, *Proc. Natl. Acad. Sci. U.S.A. 80*, 726−30.
16. Lindahl, E., Hess, B., and Spoel, D. v. d. (2001) GROMACS 3.0: A package for molecular simulation and trajectory analysis, *J. Mol. Model. 7*, 306−17.
17. Dunham, T. D., and Farrens, D. L. (1999) Conformational changes in rhodopsin. Movement of helix f detected by site-specific chemical labeling and fluorescence spectroscopy, *J. Biol. Chem. 274*, 1683−90.
18. Struthers, M., Yu, H., Kono, M., and Oprian, D. D. (1999) Tertiary interactions between the fifth and sixth transmembrane segments of rhodopsin, *Biochemistry 38*, 6597−603.
19. Gouldson, P. R., Kidley, N. J., Bywater, R. P., Psaroudakis, G., Brooks, H. D., Diaz, C., Shire, D., and Reynolds, C. A. (2004) Toward the active conformations of rhodopsin and the β2-adrenergic receptor, *Proteins 56*, 67−84.
20. Altenbach, C., Cai, K., Klein-Seetharaman, J., Khorana, H. G., and Hubbell, W. L. (2001) Structure and function in rhodopsin: Mapping light-dependent changes in distance between residue 65 in helix TM1 and residues in the sequence 306−319 at the cytoplasmic end of helix TM7 and in helix H8, *Biochemistry 40*, 15483−92.
21. Altenbach, C., Klein-Seetharaman, J., Cai, K., Khorana, H. G., and Hubbell, W. L. (2001) Structure and function in rhodopsin: Mapping light-dependent changes in distance between residue 316 in helix 8 and residues in the sequence 60−75, covering the cytoplasmic end of helices TM1 and TM2 and their connection loop CL1, *Biochemistry 40*, 15493−500.
22. Bower, M. J., Cohen, F. E., and Dunbrack, R. L., Jr. (1997) Prediction of protein side-chain rotamers from a backbone-dependent rotamer library: A new homology modeling tool, *J. Mol. Biol. 267*, 1268−82.
23. Samudrala, R., and Moult, J. (1998) An all-atom distance-dependent conditional probability discriminatory function for protein structure prediction, *J. Mol. Biol. 275*, 895−916.
24. Pappu, R. V., Marshall, G. R., and Ponder, J. W. (1999) A potential smoothing algorithm accurately predicts transmembrane helix packing, *Nat. Struct. Biol. 6*, 50−5.
25. Palczewski, K., Kumasaka, T., Hori, T., Behnke, C. A., Motoshima, H., Fox, B. A., Le Trong, I., Teller, D. C., Okada, T., Stenkamp, R. E., Yamamoto, M., and Miyano, M. (2000) Crystal structure of rhodopsin: A G protein-coupled receptor, *Science 289*, 739−45.
26. Schertler, G. F. (2005) Structure of rhodopsin and the metarhodopsin I photointermediate, *Curr. Opin. Struct. Biol. 15*, 408−15.
27. Frimurer, T. M., and Bywater, R. P. (1999) Structure of the integral membrane domain of the GLP1 receptor, *Proteins 35*, 375−86.
28. Gorn, A. H., Rudolph, S. M., Flannery, M. R., Morton, C. C., Weremowicz, S., Wang, T. Z., Krane, S. M., and Goldring, S. R. (1995) Expression of two human skeletal calcitonin receptor isoforms cloned from a giant cell tumor of bone. The first intracellular domain modulates ligand binding and signal transduction, *J. Clin. Invest. 95*, 2680−91.
29. Gether, U. (2000) Uncovering molecular mechanisms involved in activation of G protein-coupled receptors, *Endocr. Rev. 21*, 90−113.
30. Christopoulos, A., Christopoulos, G., Morfis, M., Udawela, M., Laburthe, M., Couvineau, A., Kuwasako, K., Tilakaratne, N., and Sexton, P. M. (2003) Novel receptor partners and function of receptor activity-modifying proteins, *J. Biol. Chem. 278*, 3293−7.
31. Hanley, M. R., Cheung, W. T., Hawkins, P., Poyner, D., Benton, H. P., Blair, L., Jackson, T. R., and Goedert, M. (1990) The mas oncogene as a neural peptide receptor: Expression, regulation and mechanism of action, *Ciba Found. Symp. 150*, 23−46.
32. Evans, B. N., Rosenblatt, M. I., Mnayer, L. O., Oliver, K. R., and Dickerson, I. M. (2000) CGRP-RCP, a novel protein required for signal transduction at calcitonin gene-related peptide and adrenomedullin receptors, *J. Biol. Chem. 275*, 31438−43.
33. Liang, J., Adamian, L., and Jackups, R., Jr. (2005) The membrane-water interface region of membrane proteins: Structural bias and the anti-snorkeling effect, *Trends Biochem. Sci. 30*, 355−7.
34. Udawela, M., Christopoulos, G., Tilakaratne, N., Christopoulos, A., Albiston, A., and Sexton, P. M. (2006) Distinct receptor activity-modifying protein domains differentially modulate interaction with calcitonin receptors, *Mol. Pharmacol. 69*, 1984−9.
35. Langer, I., Langlet, C., and Robberecht, P. (2005) Effect of inactivating mutations on phosphorylation and internalization of the human VPAC2 receptor, *J. Mol. Endocrinol. 34*, 405−14.
36. Iida-Klein, A., Guo, J., Takemura, M., Drake, M. T., Potts, J. T., Jr., Abou-Samra, A., Bringhurst, F. R., and Segre, G. V. (1997) Mutations in the second cytoplasmic loop of the rat parathyroid hormone (PTH)/PTH-related protein receptor result in selective loss of PTH-stimulated phospholipase C activity, *J. Biol. Chem. 272*, 6882−9.
37. Tams, J. W., Knudsen, S. M., and Fahrenkrug, J. (2001) Characterization of a G protein coupling "YL" motif of the human VPAC1 receptor, equivalent to the first two amino acids in the "DRY" motif of the rhodopsin family, *J. Mol. Neurosci. 17*, 325−30.
38. Huang, Z., Chen, Y., Pratt, S., Chen, T.-H., Bambino, T., Nissenson, R. A., and Shoback, D. M. (1996) The N-terminal region of the third intracellular loop of the parathyroid hormone (PTH)/PTH-related peptide receptor is critical for coupling to cAMP and inositol phosphate/Ca^{2+} signal transduction pathways, *J. Biol. Chem. 271*, 33382−9.
39. Takhar, S., Gyomorey, S., Su, R. C., Mathi, S. K., Li, X., and Wheeler, M. B. (1996) The third cytoplasmic domain of the GLP-1[7-36 amide] receptor is required for coupling to the adenylyl cyclase system, *Endocrinology 137*, 2175−8.

40. Couvineau, A., Lacapere, J. J., Tan, Y. V., Rouyer-Fessard, C., Nicole, P., and Laburthe, M. (2003) Identification of cytoplasmic domains of hVPAC1 receptor required for activation of adenylyl cyclase. Crucial role of two charged amino acids strictly conserved in class II G protein-coupled receptors, *J. Biol. Chem. 278*, 24759−66.

41. Heller, R. S., Kieffer, T. J., and Habener, J. F. (1996) Point mutations in the first and third intracellular loops of the glucagon-like peptide-1 receptor alter intracellular signaling. *Biochem. Biophys. Res. Commun. 223*, 624−32.

BI0615801